Global Biogeochemical Cycles®

AGU ADVANCING EARTH AND SPACE SCIENCE

RESEARCH ARTICLE
10.1029/2022GB007491

Key Points:

- It is necessary to include variable phytoplankton iron quotas to properly simulate the oceanic iron, carbon, and nitrogen cycles
- Pyrogenic iron is a key soluble iron source and has first order impacts on the marine nitrogen inventory and therefore carbon cycling

Supporting Information:

Supporting Information may be found in the online version of this article.

Correspondence to:

N. A. Wiseman,
wisemann@uci.edu

Citation:

Wiseman, N. A., Moore, J. K., Twining, B. S., Hamilton, D. S., & Mahowald, N. M. (2023). Acclimation of phytoplankton Fe:C ratios dampens the biogeochemical response to varying atmospheric deposition of soluble iron. *Global Biogeochemical Cycles*, *37*, e2022GB007491. https://doi.org/10.1029/2022GB007491

Received 9 JUN 2022
Accepted 4 APR 2023

Author Contributions:

Conceptualization: J. K. Moore
Data curation: N. A. Wiseman, B. S. Twining
Formal analysis: N. A. Wiseman
Methodology: N. A. Wiseman
Resources: N. M. Mahowald
Supervision: J. K. Moore
Visualization: N. A. Wiseman
Writing – original draft: N. A. Wiseman
Writing – review & editing: N. A. Wiseman, J. K. Moore, B. S. Twining, N. M. Mahowald

Acclimation of Phytoplankton Fe:C Ratios Dampens the Biogeochemical Response to Varying Atmospheric Deposition of Soluble Iron

N. A. Wiseman[1], J. K. Moore[1], B. S. Twining[2], D. S. Hamilton[3,4], and N. M. Mahowald[4]

[1]Department of Earth System Science, University of California Irvine, Irvine, CA, USA, [2]Bigelow Laboratory for Ocean Sciences, East Boothbay, ME, USA, [3]Marine, Earth, and Atmospheric Sciences, North Carolina State University, Raleigh, NC, USA, [4]Department of Earth and Atmospheric Science, Cornell University, Ithaca, NY, USA

Abstract Dissolved iron (dFe) plays an important role in regulating marine productivity. In high nutrient, low chlorophyll regions (>33% of the global ocean), iron is the primary growth limiting nutrient, and elsewhere iron can regulate nitrogen fixation by diazotrophs. The link between iron availability and carbon export is strongly dependent on the phytoplankton iron quotas or cellular Fe:C ratios. This ratio varies by more than an order of magnitude in the open ocean and is positively correlated with ambient dFe concentrations in field observations. Representing Fe:C ratios within models is necessary to investigate how ocean carbon cycling will interact with perturbations to iron cycling in a changing climate. The Community Earth System Model ocean component was modified to simulate dynamic, group-specific, phytoplankton Fe:C that varies as a function of ambient iron concentration. The simulated Fe:C ratios improve the representation of the spatial trends in the observed Fe:C ratios. The acclimation of phytoplankton Fe:C ratios dampens the biogeochemical response to varying atmospheric deposition of soluble iron, compared to a fixed Fe:C ratio. However, varying atmospheric soluble iron supply has first order impacts on global carbon and nitrogen fluxes and on nutrient limitation spatial patterns. Our results suggest that pyrogenic Fe is a significant dFe source that rivals mineral dust inputs in some regions. Changes in dust flux and iron combustion sources (anthropogenic and wildfires) will modify atmospheric Fe inputs in the future. Accounting for dynamic phytoplankton iron quotas is critical for understanding ocean biogeochemistry and projecting its response to variations in atmospheric deposition.

1. Introduction

Ocean biogeochemistry plays a key role in the global carbon cycle through the uptake of atmospheric carbon dioxide (CO_2) and its long-term storage via the biological and solubility pumps (Volk & Hoffert, 1985). Phytoplankton help drive the biological pump by taking up dissolved inorganic carbon and nutrients and converting them to biomass via photosynthesis. The ratios of carbon to nutrients in exported organic matter have long been used to simplify biogeochemical cycles, where a fixed, extended Redfield ratio (C:N:P:Fe) is assumed (Bruland et al., 1991; Redfield et al., 1963; Twining et al., 2015). This ratio helps determine the efficiency of the biological export of carbon with respect to potentially growth-limiting nutrients. Iron is a key micronutrient in this process as it limits phytoplankton growth in regions where other nutrients, such as nitrogen and phosphorus, are readily available (Boyd et al., 2007; J. K. Moore et al., 2004). These iron-limited waters are termed high nutrient, low chlorophyll (HNLC) regions and comprise >33% of the surface ocean (C. M. Moore et al., 2013; J. K. Moore et al., 2002; Ustick et al., 2021). Nitrogen-fixing diazotrophs are likely to be iron stressed over much of the oligotrophic ocean, linking carbon, nitrogen, and iron cycling in the tropics (Buchanan et al., 2019; Falkowski, 1997; J. K. Moore & Doney, 2007).

However, a wide range of iron to carbon (Fe:C) ratios have been observed in both sinking organic matter and in situ phytoplankton cells, complicating our understanding of the interactions between iron and carbon biogeochemistry (Fung et al., 2000; King et al., 2012). Constraining these nutrients to carbon ratios within models is necessary to properly investigate how ocean carbon cycling will interact with perturbations to nutrient cycling in a changing climate. One expected such perturbation is atmospheric iron deposition, which is sensitive to both climate change and anthropogenic activities, including fossil fuel and biomass burning (Hamilton, Scanza, et al., 2020). Thus, it is important to understand how plankton Fe:C ratios will respond to changing environmental conditions for future projections of ocean biogeochemistry.

Initial measurements of phytoplankton iron quotas relied on either radioisotope uptake experiments or bulk, size fractionation measurements using graphite furnace atomic absorption spectrometry and more recently, inductively coupled plasma mass spectrometry (Ho et al., 2003; Martin & Knauer, 1973; Schmidt & Hutchins, 1999; Sunda & Huntsman, 1995). However, these types of measurements each have some limitations. Radioisotope uptake experiments derive cellular Fe:C from uptake rates or at steady state, both of which may be impacted by potential bottle effects and rely on the addition of dissolved radiolabeled iron, which may lead to ratios that are not representative of the in situ biogenic quotas (King et al., 2012). Bulk size fractionation analysis via graphite furnace atomic absorption spectrometry and inductively coupled plasma mass spectrometry relies on measurements of the entire size class, which may be skewed by mineral and detrital particles (King et al., 2012). These methods were also unable to detect low cellular iron concentrations due to detection limits and were unable to provide information on individual taxa versus entire community assemblages (Twining et al., 2003). Single-cell synchrotron X-ray fluorescence is a relatively newer method where individual cells are isolated and individually measured for their iron and phosphorus reservoirs, while cellular carbon is estimated from cell volume (Twining et al., 2003, 2015).

Fe:C uptake by phytoplankton is primarily controlled by dissolved iron (dFe) availability in HNLC regions where nitrogen and phosphorus are replete (Sunda & Huntsman, 1995). Measurements of individual taxa iron requirements have found high variation between groups, where coastal species can vary more than 100-fold (2–200 μmol Fe/mol C), while open ocean species vary by about a factor of 20 (10–200 μmol Fe/mol C) (Marchetti & Maldonado, 2016; Sunda et al., 1991). Some coastal phytoplankton and oceanic diatoms continue to accumulate iron under iron replete conditions—up to 70 times higher than is needed to reach their maximum growth rate, suggesting that they are capable of luxury storage (Marchetti et al., 2009; Sunda & Huntsman, 1995; Twining et al., 2021). Differences in uptake rates between species are largely attributed to variations in cell surface area, where uptake rate is a function of the surface area to volume ratio and therefore smaller cells are more efficient at iron uptake due to the diffusive limitation of transport (Hudson & Morel, 1990; Morel et al., 1991; Sunda & Huntsman, 1995; Twining et al., 2004). Smaller prokaryotic cells may also use siderophore-bound iron in order to increase their uptake, potentially leading to higher Fe:C ratios than larger eukaryotes in low-Fe settings, although some species of diatoms have also been found to use iron complexed to siderophores (Kazamia et al., 2018; Sunda & Huntsman, 1995; Twining et al., 2004). Some variation in iron requirements between taxa has also been attributed to the specialized needs of certain groups. For example, nitrogen fixers such as *Trichodesmium* need iron for the nitrogenase enzyme that is required in order to reduce dinitrogen, and have been found to contain highly variable iron quotas, with Fe:C ratios ranging from 22 to 480 μmol Fe/mol C (Berman-Frank et al., 2001; Howard & Rees, 1996; Sañudo-Wilhelmy et al., 2001). Phytoplankton community composition can strongly influence the strength of the biological pump as different phytoplankton groups dominate under different conditions and have varying export efficiencies (Buesseler, 1998; Hamilton, Moore, et al., 2020). It is therefore important to accurately represent both the community composition and the nutrient requirements of the community to understand ocean carbon cycling.

Nitrogen fixers such as *Trichodesmium* are capable of converting dinitrogen gas (N_2) to a biologically useable form, ammonium (NH_4^+). These marine nitrogen fixers are integral to the marine environment, where other autotrophs are primarily nitrogen limited, and represent a significant contribution to the marine nitrogen budget, with global rates of nitrogen fixation between 125 and 223 $TgNyr^{-1}$ (Wang et al., 2019). However, the growth of the nitrogen fixers is limited by phosphorus and iron availability (Mills et al., 2004; J. K. Moore et al., 2004). Therefore, the productivity of these nitrogen-fixers represents a key link between the carbon and nitrogen cycles (Buchanan et al., 2019). Nitrogen and carbon cycles are also linked through fixed nitrogen removal via heterotrophic denitrification and anaerobic ammonium oxidation (anammox). Heterotrophic denitrification is the sequential microbial reduction of nitrate (NO_3^-) to N_2, and anammox is the chemoautotrophic oxidation of ammonium to N_2. Within the water column, these primarily occur where organic particles sink through oxygen minimum zones (Kalvelage et al., 2013), with global nitrogen loss rates estimated between 55 and 73 $TgNyr^{-1}$ (Wang et al., 2019). This process connects the rates of particulate matter export to the global nitrogen cycle, as greater export above oxygen minimum zones leads to greater rates of denitrification, and therefore, a greater loss of fixed nitrogen from the marine environment. Iron availability limits the growth of diazotrophs and modifies the sinking flux of organic matter into the oxygen minimum zones (OMZs). Thus, there are strong links and feedbacks between iron deposition, nitrogen cycling, and the marine carbon cycle (Buchanan et al., 2019; Hamilton, Moore, et al., 2020; Krishnamurthy et al., 2010; J. K. Moore & Doney, 2007).

Limited field observations have shown that phytoplankton Fe:C is generally elevated in regions of higher ambient iron concentrations. In the North Atlantic subtropical gyre, under the North African dust plume transport pathway, phytoplankton Fe:C can reach upward of 90 μmol/mol (Twining et al., 2015). Ratios also tend to be higher in coastal regions, where there is a significant continental shelf iron source due to shallower depths. These ratios tend to be lower in more remote regions that have lower atmospheric iron inputs, such as in the Indian subtropical gyre and the Southern Ocean, where ratios tend to be in the 3–15 μmol/mol range (Hopkinson et al., 2013; Twining et al., 2019).

Using fixed Redfield values for the C:N and C:P of phytoplankton in ocean models has been found to underestimate carbon fluxes or overestimate nutrient fluxes, especially in oligotrophic, strongly nutrient-limited regions (Buchanan et al., 2018; Galbraith & Martiny, 2015; Kwiatkowski et al., 2018; Moreno et al., 2018; Schneider et al., 2004; Tanioka & Matsumoto, 2017; Weber & Deutsch, 2012). About half of the CMIP6 models account for variable Fe:C ratios, while the others assume a fixed stoichiometry (Séférian et al., 2020). Few studies have investigated the impacts of variable iron stoichiometry in climate scenarios. Buitenhuis and Geider (2010) developed an iron-light colimitation model for phytoplankton growth, which allowed for the luxury uptake of Fe. This has been implemented in the ocean biogeochemical model PISCES-v2 and allows for phytoplankton iron to carbon ratios up to 40 μmol Fe/mol C (Aumont et al., 2015). Recent work with PISCES found that the linking of the iron and carbon cycles via biological Fe:C is key to controlling nutrient limitation patterns in the future ocean, with direct impacts on net primary productivity, particularly in the equatorial Pacific (Tagliabue et al., 2020). Another study using the PISCES model connected the role of diatoms with variable iron quotas to enhanced carbon export in the Southern Ocean and pointed out the necessity of further constraining diatom physiology in this region (Person et al., 2018). Variations in atmospheric iron input strongly impact spatial patterns of phytoplankton growth limitation and the areal extent of the HNLC regions at the global scale (Hamilton, Moore, et al., 2020; Krishnamurthy et al., 2010; Tagliabue et al., 2020). It may therefore be necessary to include variable iron ratios in ocean models to accurately predict the biogeochemical responses to future climate change.

The primary sources of iron to the oceans are from atmospheric deposition, terrestrial runoff and rivers, continental shelf sediments, and hydrothermal vent systems (Tagliabue et al., 2017). In the subtropical and tropical oceans, atmospheric deposition tends to be the primary source of bioavailable iron, while in the polar regions, the relative importance of continental shelf and hydrothermal vent dust likely increases (J. K. Moore & Braucher, 2008; Tagliabue et al., 2017). Atmospheric iron deposition can represent more than 50% of the iron inputs to the euphotic zone in many regions (Krishnamurthy et al., 2010). This atmospheric iron deposition is composed of two primary components: desert mineral dust and pyrogenic aerosols (Hamilton, Scanza, et al., 2020; Mahowald et al., 2011). The FeMIP model intercomparison project reported atmospheric iron deposition over a very wide range of 1.4–32.7 Gmol Fe yr^{-1} imposed in current ocean models, reflecting large uncertainties in this key ocean forcing (Tagliabue et al., 2016).

Only a fraction of the iron in the dust and pyrogenic aerosols is soluble upon deposition to the oceans. The solubility percentage of iron within desert mineral dust is highly uncertain, with estimates ranging from 1% to as high as 12%, with ocean biogeochemical models having previously often assumed constant 1%–2% solubility of the iron from dust sources (Archer & Johnson, 2000; Bopp et al., 2003; Fung et al., 2000; Jickells & Spokes, 2001; Lefèvre & Watson, 1999; Mahowald et al., 2009; Wu & Boyle, 2002). Conversely, iron from pyrogenic sourced aerosols may be more soluble and despite making up a smaller fraction of the total deposition, could potentially represent a significant portion of soluble iron deposition in many regions (Hamilton, Scanza, et al., 2020; Ito et al., 2019; Matsui et al., 2018; Sedwick et al., 2007). Recent atmospheric iron model intercomparison studies have shown that including this pyrogenic sourced iron is key to simulating observations of variations in iron solubility over the global ocean and that iron from pyrogenic wildfire sources stimulates the biological pump at a greater rate than iron from mineral dust (Hamilton, Scanza, et al., 2020; Ito et al., 2019, 2020; Myriokefalitakis et al., 2018). However, there are large uncertainties in constraining these pyrogenic sources in terms of their sources, solubilities, and fluxes, and previous estimates of pyrogenic sourced iron may be significantly underestimated (Conway et al., 2019; Hamilton et al., 2022; Lamb et al., 2021; M. Liu et al., 2022).

Here we seek to address several key questions regarding the links and feedback between variable phytoplankton Fe:C ratios and marine biogeochemical cycling. What is the relationship between phytoplankton Fe:C ratios and ambient dFe concentrations? What are the impacts of variable phytoplankton Fe:C ratios on marine biogeochemical cycling? We compare model implementations with fixed, weakly varying, and strongly varying Fe:C

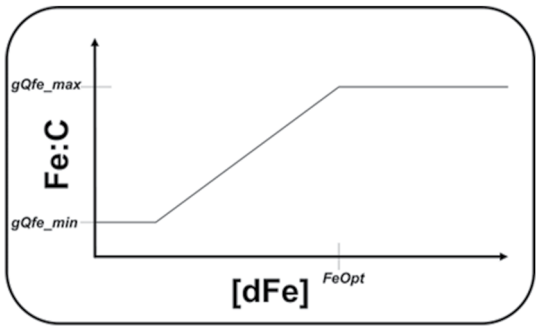

Figure 1. Phytoplankton Fe:C ratio for new growth as a function of dissolved iron. FeOpt determines the dissolved ambient iron concentration at which phytoplankton Fe:C reaches its maximum value (gQFe_max). Fe:C varies linearly with dissolved iron concentration between the prescribed, group-specific maximum (gQFe_max) and minimum (gQfe_min) quotas.

ratios, evaluating against observational data sets. We also examine how the incorporation of dynamic Fe:C ratios influences the marine biogeochemical response to variations in atmospheric deposition of soluble iron. We combined estimated depositions of pyrogenic and dust sourced iron in different ways to provide a wide range in soluble iron inputs from the atmosphere (1.5–7.0 Gmol Fe/yr). Generating the deposition estimates in this manner also allowed for some assessment of the relative biogeochemical impacts of the pyrogenic and dust sourced iron.

2. Methods

We use the Community Earth System Model (CESM) ocean circulation, marine ecosystem and biogeochemistry components. The version used is modified from CESM v1.21 but includes most science modifications that were introduced in CESM v2.0, including variable phytoplankton phosphorus quotas and an explicit ligand and iron model (Long et al., 2021; Wang et al., 2019). The model contains three explicit phytoplankton groups: diatoms, nano- to pico-sized phytoplankton (a fraction of which is assigned an implicit calcifier group) and diazotrophs (Long et al., 2021; J. K. Moore et al., 2004). The rate of nitrogen fixation by diazotrophs is proportional to their carbon fixation, where the amount fixed is the demand left after their uptake of nitrate and ammonium is calculated. The rate of denitrification is proportional to the amount of particulate organic carbon (POC) and dissolved organic carbon being remineralized in low oxygen conditions. When oxygen concentration is <5 μM, nitrate is consumed rather than oxygen during the remineralization of this organic matter (J. K. Moore & Doney, 2007). The model has one class of explicit, iron-binding ligands and external iron sources from atmospheric deposition (pyrogenic and mineral dust sourced iron), marine sediments, hydrothermal vents, and riverine inputs (Long et al., 2021; J. K. Moore & Braucher, 2008). We ran the simulations with constant pre-industrial CO_2 for 300 years and averaged the results over the last 20 years of the simulation.

The iron uptake rate and the Fe:C for new growth of these groups are a function of ambient iron concentration and a prescribed half-saturation constant, but vary only within a narrow range (2.5–6 μmol Fe/mol C) for small phytoplankton and diatoms, and 14–48 μmol Fe/mol C for the diazotrophs (J. K. Moore et al., 2004). Here, we test a much wider range of Fe:C ratios. The cellular iron to carbon ratio for new growth (gQfe) is assumed to be a linear function of the ambient dissolved iron concentration (Sunda & Huntsman, 1995). FeOpt is the group-specific, dissolved iron concentration where the Fe:C reaches its maximum value; above this concentration, the Fe:C for new growth is set at the prescribed maximum value (gQfe_max). When dissolved iron concentrations fall below FeOpt, the Fe:C for new growth decreases linearly with iron concentration proportional to FeOpt until the prescribed minimum value is reached (gQfe_min), which is imposed at lower dFe concentrations:

$$\mathrm{gQfe} = \min\left(\mathrm{gQfe\_max}, \max\left(\mathrm{gQfe\_min}, \mathrm{gQfe\_max} \cdot \frac{\mathrm{dFe}}{\mathrm{FeOpt}}\right)\right) \quad (1)$$

where gQfe is the Fe:C ratio for new growth, gQfe_max is the prescribed maximum Fe:C, gQfe_min is the prescribed minimum Fe:C, dFe is the local concentration of dissolved iron, and FeOpt is the iron concentration where Fe:C reaches its maximum value (Figure 1). The iron concentration where the minimum is reached is therefore dependent on the prescribed FeOpt, gQfe_max, and gQfe_min values, and can be calculated by the following:

$$\mathrm{dFe\_min} = \mathrm{FeOpt} \cdot \frac{\mathrm{gQfe\_min}}{\mathrm{gQfe\_max}} \quad (2)$$

$$\mathrm{VFe} = \frac{\mathrm{dFe}}{\mathrm{dFe} + \mathrm{kFe}} \quad (3)$$

Phytoplankton growth rate is calculated according to Liebig's law of the minimum, where the relative uptake rate for each nutrient (Equation 3, N, P, Fe, Si, ranging from 0 to 1) is calculated, and the lowest value determines the relative growth rate, after which temperature and light are also considered multiplicatively. Phytoplankton

growth limitation due to iron is therefore dependent on the ambient iron concentration and the iron half-saturation constant for each plankton group. We assume a fixed, minimal value for the zooplankton Fe:C of 3.0 μmol Fe/mol C, with excess ingested iron routed to dissolved iron via excretion. The Fe:C ratio of the phytoplankton is passed to the sinking export generated by aggregation and grazing. Zooplankton mortality provides additional export with low endmember Fe:C. Thus, the Fe:C ratio in the sinking biogenic export has an Fe:C value typically lower than the phytoplankton at that location. However, if scavenged iron is included, the sinking Fe:C is always higher than the phytoplankton Fe:C.

We test applying a broader range of Fe:C ratios, specific for each phytoplankton group, based on our compiled database of field observations (Table S1 in Supporting Information S1) of phytoplankton Fe:C where ambient dissolved iron was also measured (n = 142), including unpublished Arctic data from the Twining lab (Abraham et al., 2000; Hopkinson et al., 2013; King et al., 2012; Maldonado & Price, 1999; McKay et al., 2005; Sañudo-Wilhelmy et al., 2001; Sarthou et al., 2008; Schmidt & Hutchins, 1999; Tovar-Sanchez et al., 2003; Twining et al., 2004, 2010, 2011, 2015, 2019, 2021). These observations include bulk Fe:C as well as individual phytoplankton Fe:C for small phytoplankton, diatoms, and nitrogen fixers (Table S1 in Supporting Information S1). Based on these observations, we test a range of maximum Fe:C ratios for new growth (gQFe_max) from 6.0 to 120 μmol Fe/mol C (12–240 μmol Fe/mol C for diazotrophs, intervals of 10 μmol Fe/mol C) as well as a range of FeOpt values from 1.25 to 2.0 nM (1.25, 1.4, 1.6, 1.75, and 2.0 nM specifically) for each phytoplankton group. We use an optimal maximum gQFe_max of 90 μmol Fe/mol C (180 μmol Fe/mol C for diazotrophs) and an FeOpt of 1.75 nM for all phytoplankton groups based on this tuning, where we aimed to best represent the observations of phytoplankton Fe quotas. Varying these parameters had little to no impact on globally integrated NPP or POC Export, varying between 52.6–52.7 and 8.36–8.46 PgC/yr, respectively. We also compare to observed global distributions of nutrients including iron, nitrogen, and phosphorus, where nitrogen and phosphorus are from the World Ocean Atlas (Garcia et al., 2019). Observational iron data are largely from the GEOTRACES project, supplemented with historical data compilations (GEOTRACES, 2021; J. K. Moore & Braucher, 2008; Tagliabue et al., 2012).

In order to investigate the impacts of variable plankton Fe:C stoichiometry on the coupling of the iron and carbon cycles, we compare simulations with the optimized variable Fe quota model with simulations using fixed Fe:C values of 3.0, 5.0, 7.0, and 10.0 μmol Fe/mol C. We also compare variable versus fixed quotas in response to different levels of atmospheric iron deposition. We conducted a series of experiments with four different atmospheric iron deposition fields: pyrogenic Fe only, dust Fe only, dust + pyrogenic Fe, and dust Fe + pyrogenic Fe deposition where the solubility of the pyrogenic iron is doubled to account for uncertainties in the pyrogenic solubility (Hamilton, Scanza, et al., 2020). The dust deposition was extracted from the CMIP6 CESM2 historical simulation, averaged over the years 1990–2009 (Long et al., 2021). We assume that the mineral dust is 3.5% iron by weight and apply spatially varying solubility for the aerosol iron at deposition. The ratio of coarse/fine dust at deposition is a useful proxy for the distance traveled from the mineral dust source regions, as the coarse dust particles are expected to be removed more quickly during atmospheric transport. The dust iron solubility in CESM2 is a function of the ratio of coarser dust particle deposition/finer dust particle deposition (Long et al., 2021). The approach gives low solubilities near dust sources (~0.5%) increasing to greater than 10% in the most remote regions in the central Pacific, capturing the observed relationship between deposition rate and iron solubility seen in observations (Sholkovitz et al., 2012). Here, we use a recently optimized version of the relationship between the dust deposition large/small ratio and solubility. The deposition of iron from pyrogenic sources used includes soluble iron from wildfires and anthropogenic emissions with month-to-month seasonality (Hamilton, Moore, et al., 2020), here scaled up from 1.37 to 1.5 Gmol Fe yr^{-1}. The deposition assumes a constant solubility in pyrogenic aerosols of 5%, which is in the lower range of previous estimates. We include a scenario where pyrogenic aerosols have a constant solubility of 10%, which is closer to estimates from the CAM6 model, where wildfire sourced iron has a solubility of 18.8% and anthropogenic iron has a solubility of 11.2% (Hamilton, Moore, et al., 2020; Hamilton, Scanza, et al., 2020). CESM2 currently simulates pyrogenic iron in a simpler manner, relating pyrogenic iron deposition to black carbon deposition in the model (Long et al., 2021).

We force the ocean model with the pyrogenic soluble iron deposition combined with the soluble iron deposition from mineral dust in our optimal case. We include sensitivity experiments where we force the ocean model with only the pyrogenic-sourced iron and with only the dust-sourced iron. The global rate of soluble iron deposition for the pyrogenic and dust sources to the surface ocean is 1.5 and 4.0 Gmol Fe yr^{-1}, respectively, resulting in a total global deposition of 5.5 Gmol Fe yr^{-1}. A fourth sensitivity experiment combines the dust iron with the

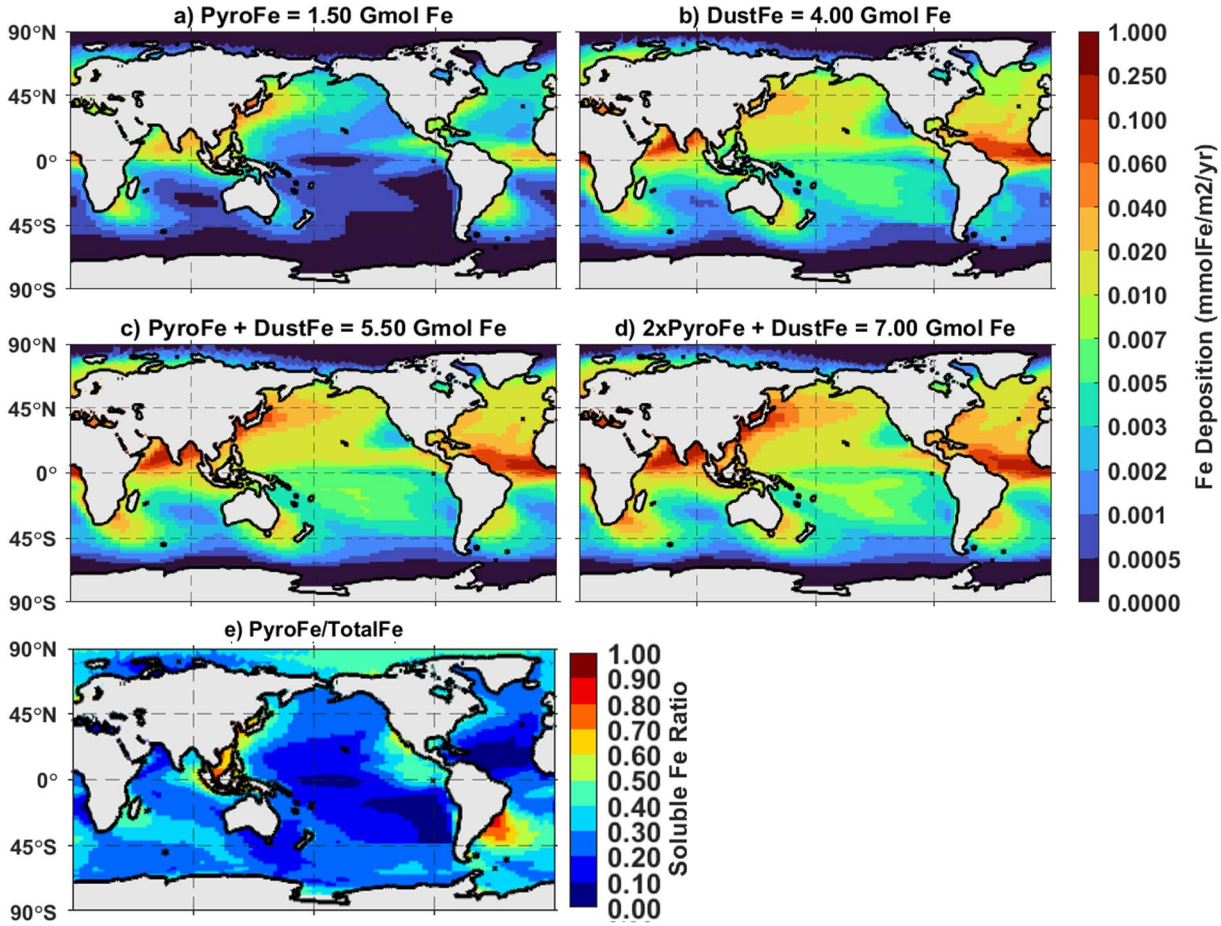

Figure 2. Atmospheric soluble iron deposition fields used to force the ocean biogeochemistry model. (a) PyroFe includes soluble iron from wildfires and anthropogenic combustion for an annual ocean surface deposition of 1.50 Gmol Fe (Hamilton, Moore, et al., 2020). (b) DustFe includes soluble iron from lithogenic sources for an annual ocean surface deposition of 4.00 Gmol Fe. (c) Annual ocean surface soluble iron deposition from pyrogenic and lithogenic sources totaling 5.50 Gmol Fe. (d) Annual ocean surface soluble iron deposition from pyrogenic and lithogenic sources where the pyrogenic solubility is doubled for a total deposition of 7.00 Gmol Fe. (e) Ratio of pyrogenic sourced iron deposition from wildfires and anthropogenic combustion divided by total soluble iron deposition from pyrogenic sources and mineral dust.

pyrogenic-sourced iron globally scaled by a factor of two (total 7.0 Gmol Fe yr^{-1}), to account for uncertainties in the solubility and aerosol source strengths, which may be greater than the initial pyrogenic-sourced iron estimate (Figure 2). One goal is to evaluate the importance of the pyrogenic iron source in driving marine biogeochemistry. These experiments provide a wide range of estimates of the atmospheric deposition of soluble iron to the oceans (1.5–7.0 Gmol Fe yr^{-1}). Each experiment was performed with the optimal, variable Fe:C stoichiometry range of 3–90 μmol Fe/mol C (6–180 μmol Fe/mol C for the diazotrophs) as well as with a fixed Fe:C stoichiometry at a value of 7 μmol Fe/mol C, for comparison.

Note that the pyrogenic soluble iron deposition exceeds the dust iron inputs considerably in the eastern and western North Pacific and in the western South Atlantic and exceeds 10% of the total soluble iron deposition everywhere but the North Atlantic subtropical gyre and the most remote Pacific regions (Figure 2e).

3. Results

We find that a broad Fe:C range for new growth (3–90 μmol Fe/mol C for the small phytoplankton and diatoms and a range of 6–180 μmol Fe/mol C for diazotrophs) best reproduces the patterns in field observations of phytoplankton Fe:C versus surface iron concentration, increasing the overall skill of the model (Figure 3). CESM previously had varying Fe:C within a limited range of 2.5–6 μmol Fe/mol C for diatoms and small phytoplankton and 14–48 μmol Fe/mol C for diazotrophs (J. K. Moore et al., 2004). Each group has an optimal dFe concentration

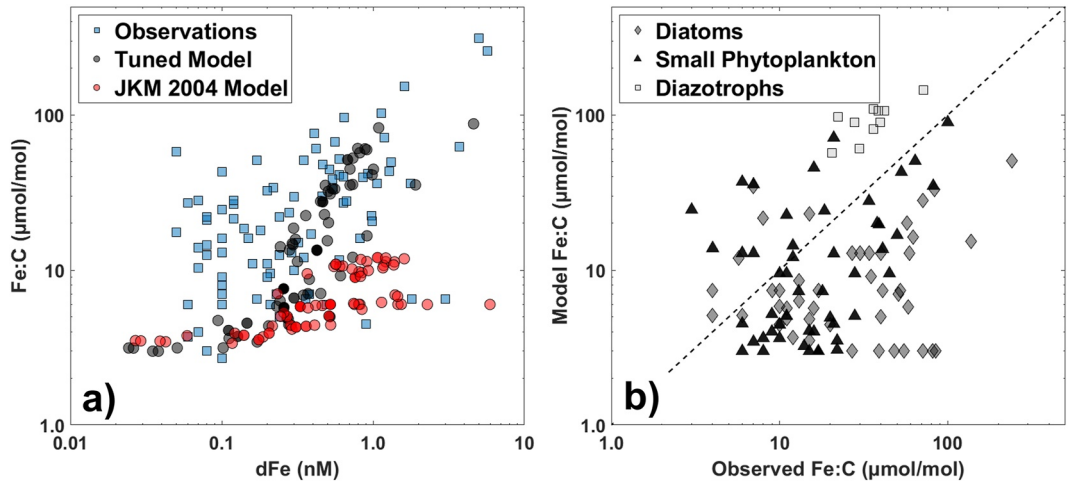

Figure 3. Comparison of field observations and simulated Fe:C of phytoplankton and ambient dFe concentrations (a) and phytoplankton Fe:C in observations and simulations (b). Observed community Fe:C as a function of dFe (a, blue squares), tuned model Fe:C versus dFe (a, gray circles), previous model Fe:C versus dFe (a, red circles) extracted from the same locations as the field observation. Observations Spearman's correlation $r_s = 0.45$, $p << 0.05$ (1e−5), tuned model $r_s = 0.87$, $p << 0.05$ (5e−27), previous model $r_s = 0.83$, $p << 0.05$ (1e−22). (b) Phytoplankton group specific model Fe:C versus observed phytoplankton Fe:C (gray diamonds are diatoms $r_s = 0.13$, black triangles are small phytoplankton $r_s = 0.28$, white squares are diazotroph $r_s = 0.63$). Model estimates were paired based on location and phytoplankton type. Dashed black line in (b) represents a 1:1 fit.

for growth of 1.75 nM, so the maximum iron quotas are achieved only in the highest dFe surface concentration regions. The tuned model with these parameters is able to reproduce the observed relationship between phytoplankton Fe:C and in situ dFe, where dissolved iron concentrations increase, so do the observed Fe:C ratios (Figure 3a). In the field observations, cellular Fe:C increases roughly linearly with dissolved iron variability with both axes on a $\log_{10}$ scale (Figure 3a). The observed range of Fe:C ratios for small phytoplankton was 3–100 µmol Fe/mol C and for diatoms was 4–528 µmol Fe/mol C (King et al., 2012; Twining et al., 2019). The variable iron quota model better captures the observed relationship between Fe:C and ambient iron concentrations (Spearman's correlation r_s of Fe:C vs. dFe from observations, the tuned model, and the previous limited-range model were 0.45, 0.87, and 0.83, respectively, Figure 3a). The model Fe:C also generally agrees with the individual cell iron to carbon measurements (Figure 3b). For each individual cell measurement, we extracted model Fe:C for the same phytoplankton group at the same location. The optimized variable model better captures these individual cell Fe:C measurements compared to the limited range model and fixed model with a Fe:C ratio of 5 µmol Fe/mol C (Figure S1 in Supporting Information S1). Using the expanded variable range did not degrade the model performance matching observations of surface nitrate, phosphate, and iron (Table S2 in Supporting Information S1). When compared to World Ocean Atlas 2018, the r_s for surface nitrate (5 m depth) decreased from 0.916 to 0.909 and the root mean squared error (RMSE) decreased from 2.41 to 2.29 µM. The r_s for surface phosphate (5 m depth) increased from 0.924 to 0.928, comparing the limited-range and variable models, while the RMSE decreased from 0.188 to 0.181 µM. For iron, the r_s increased from 0.445 to 0.490 and the RMSE decreased from 1.288 to 1.265 nM.

Overall, the model is able to reproduce the observed spatial variations between the Atlantic, Pacific, and Southern Oceans (Figure 4). Phytoplankton Fe:C is elevated in regions where surface dFe is elevated due to regional inputs such as high atmospheric dust deposition, coastal shelf sources, and upwelling. Diazotroph Fe:C measurements are limited to the North Atlantic, while some small phytoplankton and diatom measurements are available for most ocean basins. However, even within a small region the model is able to replicate the gradient of decreasing Fe:C ratios for the diazotrophs, as dFe decreases from near coast to more offshore (Figure 4).

Regions where the model and observations diverge may be driven by colimitation. For example, the model underestimates diatom Fe:C in the oligotrophic southern Pacific gyre, where the observed values seem very high compared with other regions. Twining et al. (2021) suggested that nitrogen limitation may lead to increases in the cellular Fe:C ratios, as the nitrogen limitation would decrease the frequency of cell division, allowing for iron

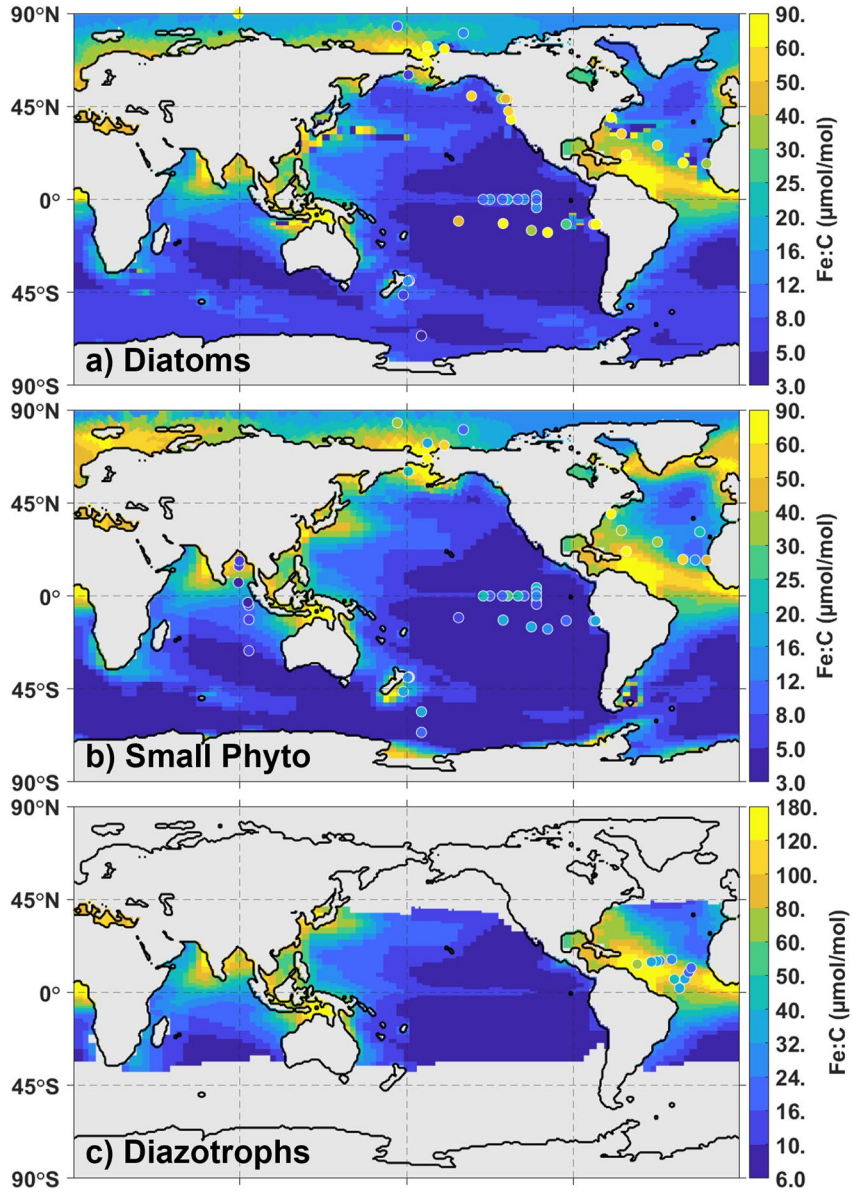

Figure 4. Optimized model patterns of (a) diatom group Fe:C overlaid with circles showing observations of diatom Fe:C ($r_s = 0.13$), (b) small phytoplankton group Fe:C overlaid with circles showing observations of small phytoplankton Fe:C ($r_s = 0.28$), and (c) diazotroph group Fe:C overlaid with circles showing observations of diazotroph Fe:C ($r_s = 0.63$).

to accumulate within diatom cells as luxury iron uptake. This is not seen in the small phytoplankton community because they are expected to maintain their growth rates even in low-nutrient regions due to their higher surface to volume ratios, and because they have much less capacity for luxury uptake and storage. Our model does not allow for luxury uptake, but rather sets the uptake proportional to current growth requirements. The r_s values for model Fe:C for each group versus the observations (small phytoplankton, diatom, diazotrophs) were 0.28, 0.13, and 0.63, respectively, for the variable quota model, while they were 0.13, 0.23, and 0.17, respectively, with the original limited-range model.

3.1. Fixed Versus Variable Fe Quotas

We find that using fixed stoichiometry in place of variable stoichiometry has first order impacts on nutrient cycling within the surface ocean. One method to quantify this impact is the HNLC index. We define an HNLC

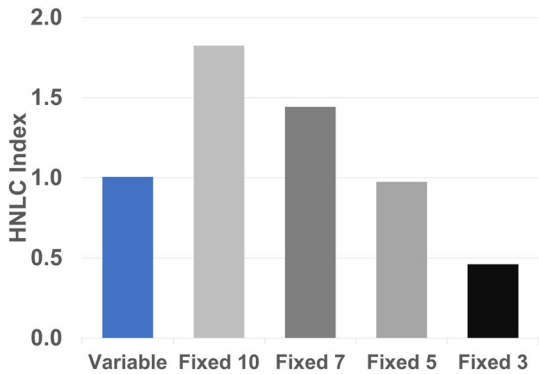

Figure 5. High nutrient, low chlorophyll (HNLC) index for four simulations within the Central Pacific HNLC region (between 25°N and 25°S, east of 150°E). Index is defined as the ratio of ocean surface area where nitrate concentrations exceed 0.3 μM in each simulation compared to the WOA18. Variable is the tuned model with variable Fe:C ranging from 3 to 90 μmol Fe/mol C for small phytoplankton and diatoms and 6–180 μmol Fe/mol C for diazotrophs, the fixed scenarios of 10, 7, 5, and 3 are where the model phytoplankton Fe:C is fixed for all groups at 10, 7, 5, and 3 μmol Fe/mol C, respectively.

region in the Pacific Ocean between 25°N and 25°S, east of 150°E, and the HNLC index as the area in the HNLC region that has surface nitrate concentrations greater than 0.3 μM in the model output, divided by the same metric for nitrate from the World Ocean Atlas 2018 (WOA18) (Garcia et al., 2019). With the expanded variable Fe:C range, we are able to reproduce the HNLC size as seen in the WOA18, with an HNLC index of 1.0063 (Figure 5). With fixed stoichiometry, the HNLC extent can be captured with a fixed Fe:C of 5 μmol/mol but expands or retracts rapidly with other fixed stoichiometries. For fixed Fe:C ratios of 3, 5, 7, and 10 μmol Fe/mol C, the HNLC areal extent changes by −54%, −2%, +44%, and +81%, respectively (Figure 5).

Comparing the fixed ratio models versus the optimized variable Fe quota model, there are modest impacts on carbon fluxes (NPP, export) integrated at the global or Central Pacific HNLC region scales (Table 1). However, there are large shifts in the spatial patterns of NPP and carbon export across the simulations, with disproportionate impacts on key fluxes within the marine nitrogen cycle. Global NPP decreased by up to 5% with fixed quotas, and NPP in the HNLC region decreased by up to 9% (Table 1). The regional NPP response to the chosen fixed value for Fe:C is non-linear, with the fixed value of 7 μmol Fe/mol C having the weakest response of a 3% decrease, while the 3 and 10 μmol Fe/mol C versions had stronger decreases of 7% and 9%. The 3 and 10 Fe:C cases have more biased Fe/C ratios relative to the observations, leading to strong regional over/underestimates of productivity and export, which influence downstream regions. The variations in HNLC size are not strongly dependent on the specific values of gQFe_max and FeOpt (Figure S2 in Supporting Information S1).

The optimized variable model, limited-range model, and fixed ratio of 5 μmol Fe/mol C, all generally reproduce observed variations in dissolved iron concentrations for the top 100 m (Figure S3 in Supporting Information S1). However, the limited variable model and the 5 μmol Fe/mol C have larger positive biases in the Saharan dust plume. In the North Atlantic from 0°N to 20°N (iron bias 0.226 nM for the variable model, 0.6578 nM for the limited-range, and 0.703 nM for fixed stoichiometry). Low, fixed Fe:C values will lead to positive iron biases in high dust regions because the biological export will be underestimated. This would lead to an overestimation of the lateral export of iron away from the high input regions.

Surface chlorophyll spatial patterns shift sharply in the tropical Pacific in response to the treatment of plankton Fe quotas (Figure 6). The optimized model is able to reproduce patterns seen in satellite chlorophyll products (log-transformed $r = 0.60$). A fixed ratio of 10 μmol Fe/mol C results in up to 60% underestimation of surface chlorophyll in the equatorial upwelling zone, while the more western region of the Pacific sees overestimates of up to 60%. This is most likely due to the excess nitrogen and phosphorus not utilized in the equatorial upwelling

Table 1
Changes in Key Annual Global and Regional Carbon Fluxes in the Optimal Model When Fixed Stoichiometry Is Used Versus the Expanded Variable Range

Fe:C	NPP (PgC/yr)	POC export (PgC/yr)	Nitrogen fixation (TgN/yr)	Water column denitrification (TgN/yr)	HNLC NPP (PgC/yr)	HNLC POC export (PgC/yr)
Variable	53.8	8.5	225.3	63.1	13.6	2.03
Fixed 10	51.2 (−5%)	8.0 (−6%)	173.1 (−23%)	20.6 (−67%)	12.4 (−9%)	1.74 (−14%)
Fixed 7	52.8 (−2%)	8.3 (−2%)	201.6 (−10%)	40.6 (−35%)	13.2 (−3%)	1.93 (−5%)
Fixed 5	53.5 (−1%)	8.5 (0%)	228.4 (+1%)	67.2 (+7%)	13.5 (−2%)	2.02 (−2%)
Fixed 3	53.3 (−1%)	8.6 (+2%)	260.6 (+15%)	102.4 (+62%)	12.7 (−7%)	1.94 (−4%)

Note. Percentages are percent change from the tuned variable model where Fe:C ranges from 3 to 90 μmol Fe/mol C for small phytoplankton and diatoms and 6–180 μmol Fe/mol C for diazotrophs. The fixed scenarios of 10, 7, 5, and 3 are where the model phytoplankton Fe:C is fixed for all groups at 10, 7, 5, and 3 μmol Fe/mol C, respectively. NPP is net primary productivity, POC is particulate organic carbon, HNLC is Central Pacific high nutrient low chlorophyll region between 25°N and 25°S, east of 150°E.

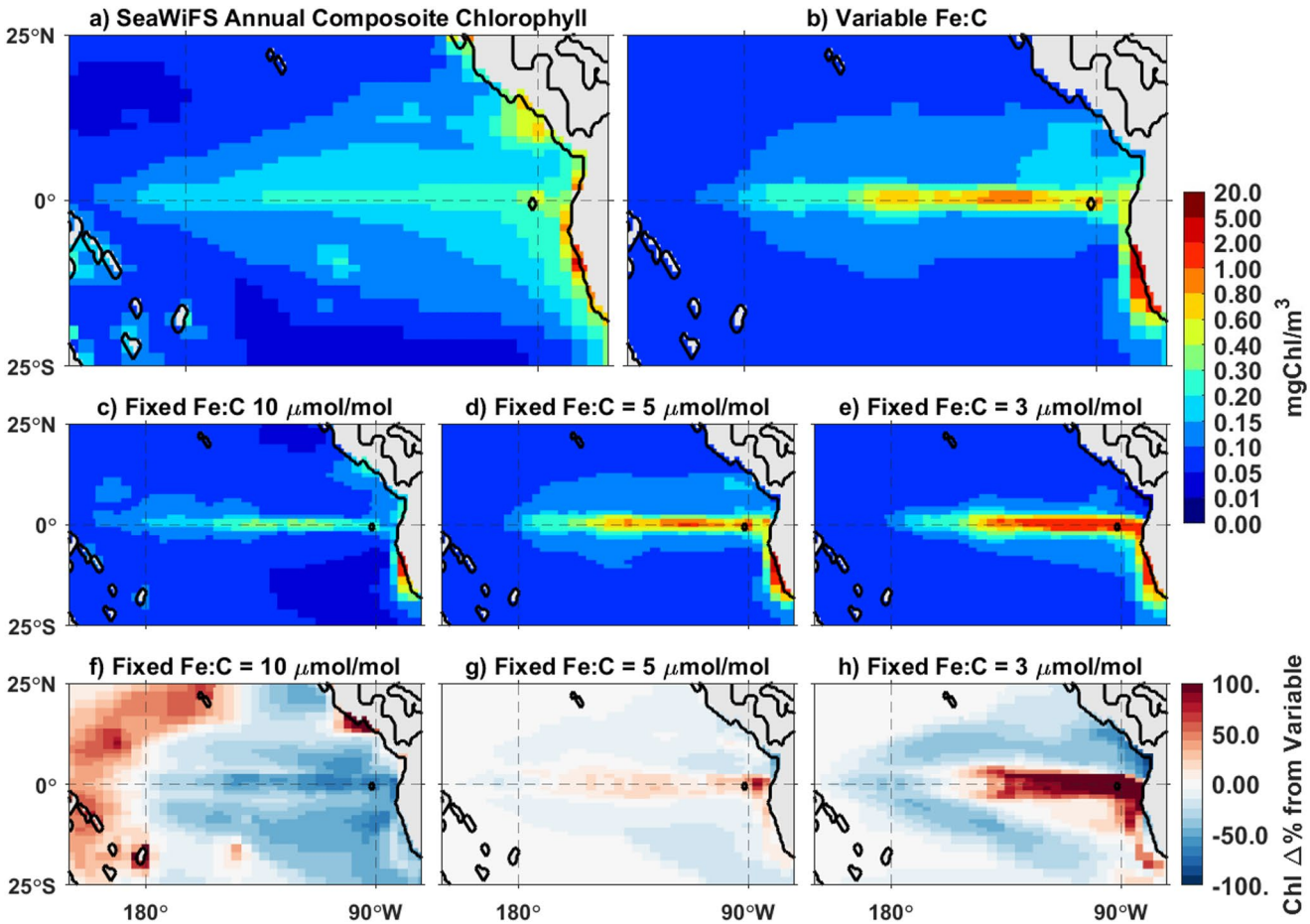

Figure 6. SeaWiFS chlorophyll climatology (a) and optimized model surface chlorophyll (b, mgChl/m^3) for our high nutrient, low chlorophyll region. Middle panels show surface chlorophyll for fixed Fe:C simulations (c–e), and bottom panels show the percent change of chlorophyll for fixed Fe:C simulations (f–h) compared to the dynamic iron quota model.

region due to the high iron requirements being transported laterally to the oligotrophic gyres increasing chlorophyll concentrations from less than 0.05 mgChl/m^3 to between 0.05 and 0.10 mgChl/m^3. In contrast, using a fixed Fe:C ratio of 3 μmol Fe/mol C results in an overestimate of chlorophyll in the equatorial upwelling tongue by greater than 100%. This is due to the increase in iron availability from the lack of efficient iron export, leading to a buildup of available iron in the surface waters. This allows for phytoplankton to increase their biomass to a greater extent than they would under stronger iron limitation, thereby driving the increase in surface chlorophyll. However, due to the reduced iron limitation, the surrounding areas transition to nitrogen limitation, resulting in a decrease in surface chlorophyll outside the equatorial upwelling tongue. The fixed ratio of 5 μmol Fe/mol C was able to reproduce a chlorophyll pattern and HNLC extent similar to the variable model, however there is much greater chlorophyll in the coastal region of the equatorial upwelling region due to the rigidity of the Fe:C ratio, similar to the 3 μmol Fe/mol C case, although to a milder extent. The variable Fe quota model, which gives high Fe:C in the plankton near the coast and very low Fe:C values in the offshore waters, is best able to replicate the satellite chlorophyll patterns. Fixed ratio models cannot match this high iron to low iron transition in the Fe:C ratio, leading to regional dissolved iron biases, as noted above for the North Atlantic.

There are also large shifts in the spatial patterns of sinking POC export in this region (Figure 7). The simulation with a fixed Fe:C of 5 μmol Fe/mol C had the pattern most similar to the variable quota model. In the 10 μmol Fe/mol C simulation, most of the sediment-sourced iron is used up nearshore, with little advection to the open ocean (Figure 7c). In contrast, with the 3 μmol Fe/mol C quota, much less iron is used up nearshore, and there is a much larger lateral flux of iron to the open ocean. These shifts in the spatial patterns of export influence the amount of organic matter sinking into the oxygen minimum zones, leading to large swings In the rates of water

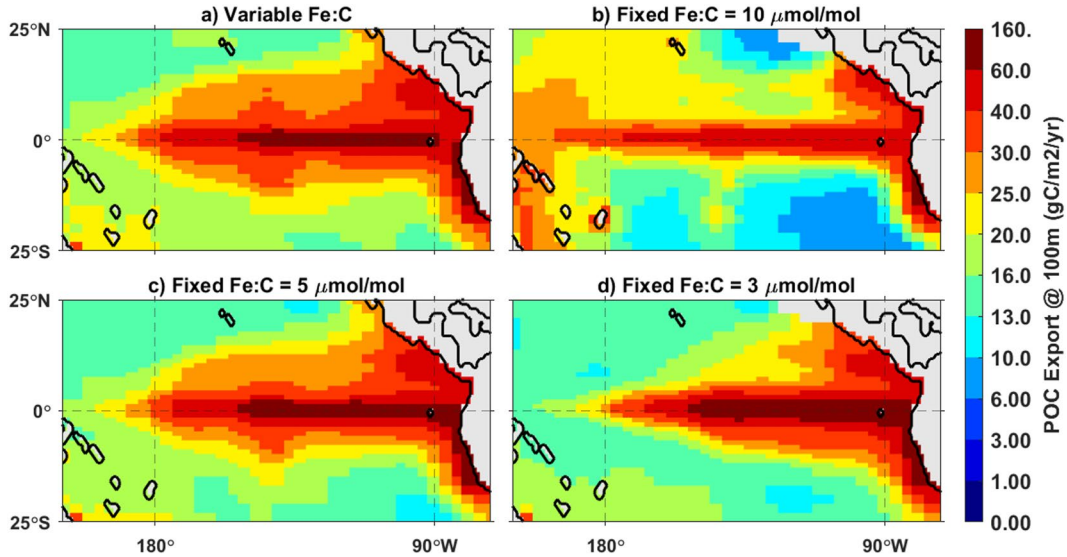

Figure 7. Sinking particulate organic carbon export at 100 m depth comparing the dynamic Fe:C model (a) and with simulations using fixed Fe:C ratios of 3, 7, and 10 μmol Fe/mol C (b–d, respectively).

column denitrification, even though the integrated POC export changes only modestly at the global or regional scale (Table 1).

Varying plankton iron quotas change the efficiency of the biological export of iron. This can have strong impacts on the spatial patterns of nutrient limitation as iron becomes exported more or less efficiently relative to the other nutrients. With a fixed Fe:C ratio of 10 μmol Fe/mol C, the iron-limited areas expand substantially compared with the variable Fe:C simulation (Figure 8). The iron-limited area for the small phytoplankton group increases from

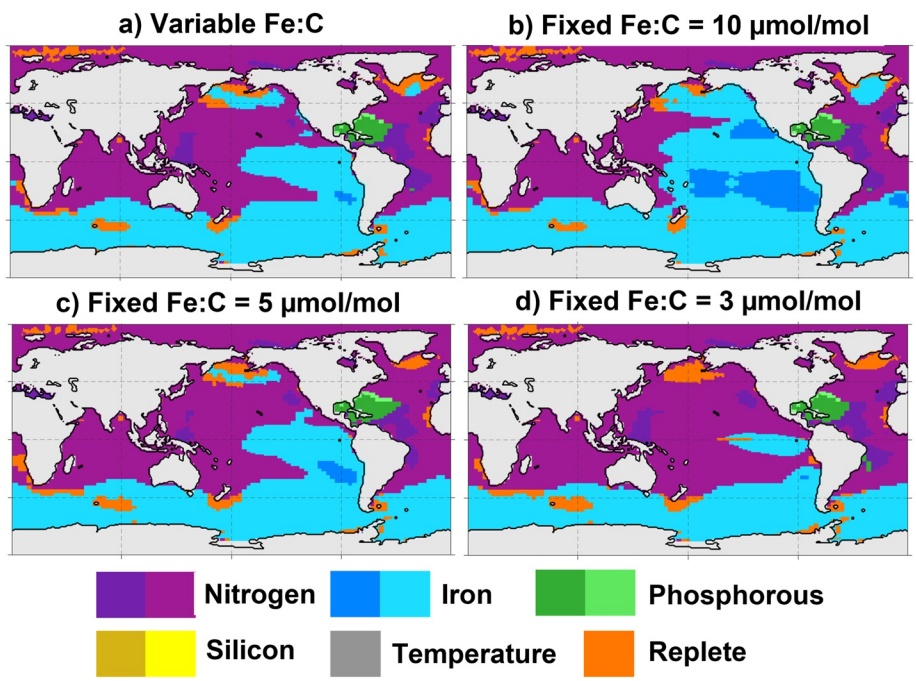

Figure 8. Patterns of nutrient limitation of small phytoplankton growth from variable and fixed iron quota simulations. Phytoplankton are nutrient replete when nutrient limitation reduces growth by less than 10%. Darker color shading indicates where growth is reduced by more than 50% from the maximum growth rate. The tuned model is shown in (a) and the simulations using fixed Fe:C ratios of 10, 5, and 3 μmol Fe/mol C (b–d) respectively.

Table 2
Percent Change in Key Carbon Fluxes for the Pyrogenic Iron Scenarios Compared to the Optimal Deposition Scenario With Variable Stoichiometry in the Equatorial High Nutrient, Low Chlorophyll Area and Globally

Deposition	Fe:C	Global NPP	Global POC export	HNLC NPP	HNLC POC export
CESM2opt	Variable	53.8 PgC	8.5 PgC	13.6 PgC	2.03 PgC
5.5 Gmol Fe/yr					
PyroFe	Variable	−7%	−9%	−15%	−21%
1.5 Gmol Fe/yr	Fixed 7	−13%	−14%	−32%	−37%
DustFe	Variable	+0.2%	−1%	+2%	+0.3%
4.0 Gmol Fe/yr	Fixed 7	−3%	−4%	−4%	−8%
DustFe + 2xPyroFe	Variable	−0.4%	+1%	−2%	−1%
7.0 Gmol Fe/yr	Fixed 7	−2%	−1%	−3%	−4%

37.4% of the total ocean area with variable Fe:C, up to 38.9% and 56.78% with the fixed Fe:C of 5 and 10 μmol Fe/mol C, respectively (Figure 8). This is because iron is already limiting in the HNLC regions, and when higher Fe:C ratios are prescribed, iron is exported more efficiently per unit carbon, resulting in even less iron being available and therefore stronger iron limitation. With a fixed ratio of 3 μmol Fe/mol C, the HNLC region outside the equatorial upwelling zone transitions from iron limitation to nitrogen limitation, as less iron is exported per mol of carbon and iron limitation is weakened. This results in the regional transition to nitrogen limitation, as nitrate supply can be readily consumed when iron is available.

3.2. Impacts of Varying Iron Deposition on Ocean Biogeochemistry

We compare simulations with variable and fixed Fe:C stoichiometry across a range of atmospheric deposition rates (1.5–7.0) Using variable stoichiometry dampens the impacts of changing iron deposition on the global ocean carbon cycle compared with fixed Fe:C (Table S2 in Supporting Information S1). At lower deposition rates, using fixed Fe:C has a larger impact on carbon cycling, with NPP 15% lower and sinking POC 51% lower when a fixed Fe:C of 10 μmol Fe/mol C is used versus the variable ratios (Table 2).

With increasing deposition, NPP and sinking POC do not respond as strongly when using variable versus fixed stoichiometry, with NPP and POC being 0.4% lower and 1% higher respectively (Table 1). There is a modest change in NPP from low deposition to high deposition (50.3–53.8 PgC/yr) when the optimal variable Fe:C is used. By having dynamic, variable iron quotas, phytoplankton are able to partially dampen, or buffer, the effects of changing iron deposition by decreasing Fe:C when iron is scarce to maintain productivity. Increasing Fe:C ratios lead to more efficient export of iron with increasing iron deposition. Thus, models with fixed Fe quotas will overestimate the biogeochemical impacts of varying iron deposition by not accounting for this phytoplankton acclimation to available nutrient concentrations.

Variations in atmospheric iron inputs have strong impacts on global nitrogen fluxes in conjunction with the fixed or optimized variable Fe quota models. When atmospheric deposition is decreased (PyroFe and DustFe simulations), both nitrogen fixation and water column denitrification decrease drastically (Figure 9). The reduction in nitrogen fixation can be attributed to the decrease in diazotroph productivity. Diazotrophs are iron limited in much of the surface ocean. Therefore, when the atmospheric deposition is decreased, diazotroph productivity is reduced, and global rates of nitrogen fixation decrease accordingly. The decrease in water column denitrification can be attributed to a general decrease in productivity and carbon export, especially in the eastern Pacific where iron is the primary limiting nutrient. This impacts the HNLC regions in particular, which increase in area by 23% when pyrogenic sourced iron is omitted, and iron limitation expands to regions that were previously nitrogen limited (Figure S4 in Supporting Information S1). With the reduction of atmospheric iron deposition and stronger iron limitation, primary productivity decreases, resulting in less organic matter sinking through the oxygen deficient zones. With less organic matter to degrade, water column denitrification drops dramatically. This feedback between iron limitation and water column denitrification is one of the key links between the iron and nitrogen cycles. Proper estimates of iron deposition are necessary in order to accurately simulate the global marine nitrogen cycle. When the optimal iron deposition field is used, the simulated global nitrogen fixation rate

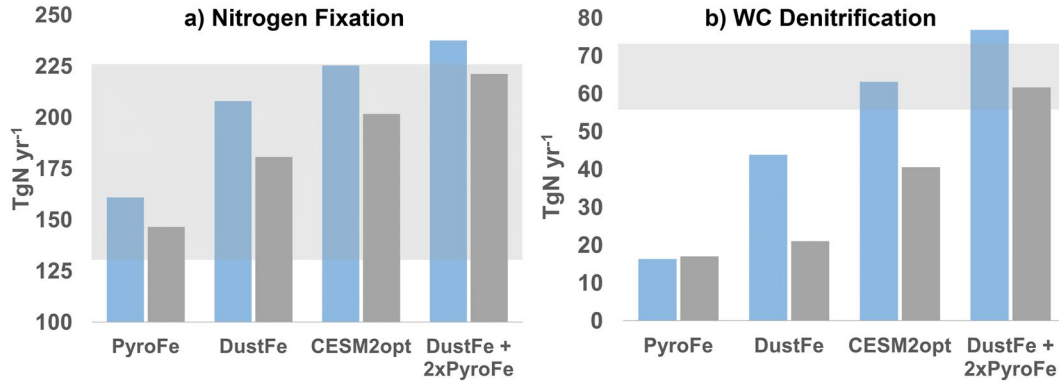

Figure 9. Global annual nitrogen fixation (a) and water column denitrification (b) under the various iron deposition scenarios for the optimized variable model (blue) and fixed Fe:C of 7 μmol Fe/mol C scenarios (dark gray). The light gray background boxes represent the estimated ranges for nitrogen fixation and water column denitrification from a recent inverse model study (Wang et al., 2019).

is 225 TgN yr^{-1}, while the global water column denitrification rate is 63 TgN yr^{-1}, which are both in agreement with recent inverse model estimates (Wang et al., 2019).

4. Conclusions

Phytoplankton Fe:C uptake links not only the oceanic iron and carbon cycles but also strongly impacts the marine nitrogen cycle as well. It is therefore important that the representation of phytoplankton iron quotas in biogeochemical models reflect the observed biological patterns. This requires not only variable quotas but also a large variable range to best represent the flexibility of these phytoplankton groups under a changing environment. We find that a range of 3–90 μmol Fe/mol C for the small phytoplankton and diatoms and a range of 6–180 μmol Fe/mol C for diazotrophs better represent the spatial variability of individual cell iron to carbon ratios between ocean basins and the observed relationship between iron to carbon ratios and dissolved iron concentrations.

Our results suggest that using a nutrient-dependent "frugal phytoplankton" approach to stoichiometry can capture some of the observed variation in phytoplankton iron to carbon ratios (Galbraith & Martiny, 2015). The expanded range is also in agreement with previous studies, such as Person et al. (2018), where expanded diatom Fe:C variability in the lower range resulted in improved model representations of surface chlorophyll in the Southern Ocean. There is considerable uncertainty in the parameter values for the maximum and minimum Fe quotas. The phytoplankton Fe:C observations provide a way to tune these parameters so ocean models can capture the observed spatial variations in Fe quotas. We expect that the exact values of the model parameters could differ across models due to differences in other factors, such as the scavenging parameterizations and the levels of external iron inputs. The HNLC index was relatively insensitive to FeOpt values between ∼1 and 2 nM (Figure S2 in Supporting Information S1). Fixed Fe:C ratio models will generate larger regional biases in surface iron concentrations and less accurate spatial patterns of nutrient limitation. Additional in situ observations are needed to better constrain these parameter values, in terms of determining the iron concentration where the community begins to acclimate to increasing iron stress by modifying their quotas.

Using the increased iron stoichiometry variability does not significantly impact the surface nutrient patterns yet leads to diverging responses to changes in soluble iron deposition. This highlights the utility of biological information such as observations of phytoplankton Fe:C ratios to informing prognostic models. While the surface nutrient fields that are typically used to tune the model parameters are not significantly impacted, we can instead use the novel information provided by the individual phytoplankton cell measurements to constrain their Fe:C ratios for growth. This approach could prove useful for other parameters within the model, as this biological information can reduce the degrees of freedom present when tuning marine ecosystem models by informing the ranges for parameters that are otherwise determined via guess and check.

The link between iron and carbon via phytoplankton Fe:C uptake has first order impacts on global nutrient cycling. When Fe:C ratios are fixed, surface nutrient distributions are impacted, particularly in regions where

atmospheric iron deposition rates are low, that is, the Pacific HNLC region, leading to changes in the primary limiting nutrient as macronutrients are drawn down or increased. This response is sensitive to the fixed value chosen, and results in significant increases or decreases in the areal extent of these regions (Figure 8). This leads to downstream effects on water column denitrification, as reductions in the POC export to the nearby oxygen minimum zones are reduced when the iron supply is not able to maintain phytoplankton growth (Table 1). The study by Person et al. (2018) focused on the ability of diatoms to maintain significant growth rates in low iron conditions, our study reaches a similar conclusion, albeit through a separate mechanism. By allowing phytoplankton iron uptake to be reduced in low iron waters via the Fe:C ratios, there is more iron left available to sustain growth, where a fixed Fe:C may overestimate the iron limitation and the growth rate reduction.

The flexibility of phytoplankton variable iron quotas is key to them maintaining productivity in regions of low deposition, as previously mentioned, but also when that deposition changes. When only dust sourced iron is used to force the model, global NPP and POC export are reduced by 3% and 4%, respectively, when fixed stoichiometry is used. However, when variable stoichiometry is used, NPP and POC exports increase by 0.2% and decrease by 1%, respectively, showing that phytoplankton are able to acclimate to changes in atmospheric deposition rates. However, this only dampens the biogeochemical response and there are limits to this acclimation as shown by the reductions in NPP and POC export when only pyrogenic sourced iron is used in both the variable and fixed scenarios, as well as the generally large impacts on nitrogen fluxes (Table S2 in Supporting Information S1).

Future changes in atmospheric iron deposition under different climate scenarios are still highly uncertain as they will be modified by climate change and anthropogenic activities (Hamilton, Moore, et al., 2020; Mahowald et al., 2009, 2011). Pyrogenic iron inputs can rival dust sources in some regions. Our results suggest that pyrogenic iron may exceed dust iron inputs in the western North Pacific and western South Atlantic (Figure 2e) We see some of the greatest impacts on carbon and nitrogen cycling under different deposition scenarios in the equatorial Pacific, where export production can directly impact denitrification rates in the OMZs and nitrogen fixation rates in the gyres. In order to make reliable projections of the interactions between marine ecosystems and the cycling of Fe, C, and N, it seems important to include the pyrogenic iron sources, which are significant in magnitude and highly variable through time. Not accounting for this source could result in underestimates of global ocean nitrogen fixation and water column denitrification, which are integral to the global ocean-fixed nitrogen inventory, and therefore carbon cycling in a primarily nitrogen-limited ocean (Buchanan et al., 2019; Hamilton, Moore, et al., 2020). Large shifts in the pyrogenic-sourced aerosols are likely in the future, responding to changes in wildfire activity and anthropogenic combustion patterns (Hamilton et al., 2022; M. Liu et al., 2022; Mahowald et al., 2009).

We used observations of phytoplankton Fe:C ratios to constrain the modeling effort. There is a great need for additional field measurements of phytoplankton elemental stoichiometry, but also stoichiometry for other ecosystem components, including within zooplankton and the sinking particulate flux, if we are to unravel the multiple processes modifying the phytoplankton stoichiometry before and after the export of organic matter from the euphotic zone. The GEOTRACES program has greatly expanded the global-scale observational data sets for iron and other trace elements (Anderson, 2020). But there are still large uncertainties regarding the marine iron cycle, including the magnitude of different sources, the rates and dynamics of removal by particle scavenging, and the cycling of the iron-binding ligands. Additional field and laboratory studies are necessary to reduce these uncertainties, and better constrain different aspects of the complex Earth System Models used for climate projection. A better understanding of the biological links between the elemental cycles is critical for understanding current patterns, but also for projecting future changes in response to climate warming and other anthropogenic activities in the future (Buchanan et al., 2019; Y. Liu et al., 2023; J. K. Moore et al., 2018).

Data Availability Statement

The simulations used in this manuscript are available as NetCDF files, while the compilation of phytoplankton iron to carbon observations is available as a .csv file via Dryad at the following: https://doi.org/10.7280/D1KQ5Q. Instructions for downloading CESM can be found at https://escomp.github.io/CESM/versions/cesm2.2/html/downloading_cesm.html.

Acknowledgments
The authors wish to thank the editor (Zanna Chase) and the two reviewers (Christoph Völker and Pearse J. Buchanan) for their thoughtful suggestions and comments. The authors wish to thank the scientists and supporters of the GEOTRACES program, which provided support for the field observations used here. J.K.M. and N.A.W. acknowledge support from the U.S. Department of Energy, Biological and Environmental Research Division, Earth System Modeling Program Grants DE-SC0016539 and DE-SC0022177. B.S.T. acknowledges support from NSF OCE-1829819 and OCE-2023237. D.S.H. and N.M.M. acknowledge support from DOE DE-SC0021302. This research used resources of the Advanced Photon Source; a U.S. Department of Energy (DOE) Office of Science user facility operated for the DOE Office of Science by Argonne National Laboratory under Contract No. DE-AC02-06CH11357.

References

Abraham, E. R., Law, C. S., Boyd, P. W., Lavender, S. J., Maldonado, M. T., & Bowie, A. R. (2000). Importance of stirring in the development of an iron-fertilized phytoplankton bloom. *Nature*, *407*(6805), 727–730. https://doi.org/10.1038/35037555

Anderson, R. F. (2020). GEOTRACES: Accelerating research on the marine biogeochemical cycles of trace elements and their isotopes. *Annual Review of Marine Science*, *12*(1), 1–37. https://doi.org/10.1146/annurev-marine-010318-095123

Archer, D. E., & Johnson, K. (2000). A model of the iron cycle in the ocean. *Global Biogeochemical Cycles*, *14*(1), 269–279. https://doi.org/10.1029/1999gb900053

Aumont, O., Ethé, C., Tagliabue, A., Bopp, L., & Gehlen, M. (2015). PISCES-v2: An ocean biogeochemical model for carbon and ecosystem studies. *Geoscientific Model Development*, *8*(8), 2465–2513. https://doi.org/10.5194/gmd-8-2465-2015

Berman-Frank, I., Cullen, J. T., Shaked, Y., Sherrell, R. M., & Falkowski, P. G. (2001). Iron availability, cellular iron quotas, and nitrogen fixation in *Trichodesmium*. *Limnology & Oceanography*, *46*(6), 1249–1260. https://doi.org/10.4319/lo.2001.46.6.1249

Bopp, L., Kohfeld, K. E., Le Quéré, C., & Aumont, O. (2003). Dust impact on marine biota and atmospheric CO_2 during glacial periods. *Paleoceanography*, *18*(2), 1046. https://doi.org/10.1029/2002pa000810

Boyd, P. W., Jickells, T., Law, C. S., Blain, S., Boyle, E. A., Buesseler, K. O., et al. (2007). Mesoscale iron enrichment experiments 1993–2005: Synthesis and future directions. *Science*, *315*(5812), 612–617. https://doi.org/10.1126/science.1131669

Bruland, K. W., Donat, J. R., & Hutchins, D. A. (1991). Interactive influences of bioactive trace metals on biological production in oceanic waters. *Limnology & Oceanography*, *36*(8), 1555–1577. https://doi.org/10.4319/lo.1991.36.8.1555

Buchanan, P. J., Chase, Z., Matear, R. J., Phipps, S. J., & Bindoff, N. L. (2019). Marine nitrogen fixers mediate a low latitude pathway for atmospheric CO_2 drawdown. *Nature Communications*, *10*(1), 4611. https://doi.org/10.1038/s41467-019-12549-z

Buchanan, P. J., Matear, R. J., Chase, Z., Phipps, S. J., & Bindoff, N. L. (2018). Dynamic biological functioning important for simulating and stabilizing ocean biogeochemistry. *Global Biogeochemical Cycles*, *32*(4), 565–593. https://doi.org/10.1002/2017gb005753

Buesseler, K. O. (1998). The decoupling of production and particulate export in the surface ocean. *Global Biogeochemical Cycles*, *12*(2), 297–310. https://doi.org/10.1029/97gb03366

Buitenhuis, E. T., & Geider, R. J. (2010). A model of phytoplankton acclimation to iron-light colimitation. *Limnology & Oceanography*, *55*(2), 714–724. https://doi.org/10.4319/lo.2010.55.2.0714

Conway, T. M., Hamilton, D. S., Shelley, R. U., Aguilar-Islas, A. M., Landing, W. M., Mahowald, N. M., & John, S. G. (2019). Tracing and constraining anthropogenic aerosol iron fluxes to the North Atlantic Ocean using iron isotopes. *Nature Communications*, *10*(1), 2628. https://doi.org/10.1038/s41467-019-10457-w

Falkowski, P. G. (1997). Evolution of the nitrogen cycle and its influence on the biological sequestration of CO_2 in the ocean. *Nature*, *387*(6630), 272–275. https://doi.org/10.1038/387272a0

Fung, I. Y., Meyn, S. K., Tegen, I., Doney, S. C., John, J. G., & Bishop, J. K. B. (2000). Iron supply and demand in the upper ocean. *Global Biogeochemical Cycles*, *14*(1), 281–295. https://doi.org/10.1029/1999gb900059

Galbraith, E. D., & Martiny, A. C. (2015). A simple nutrient-dependence mechanism for predicting the stoichiometry of marine ecosystems. *Proceedings of the National Academy of Sciences of the United States of America*, *112*(27), 8199–8204. https://doi.org/10.1073/pnas.1423917112

Garcia, H., Weathers, K., Paver, C., Smolyar, I., Boyer, T., Locarnini, M., et al. (2019). World Ocean Atlas 2018. Volume 4: Dissolved inorganic nutrients (phosphate, nitrate and nitrate+nitrite, silicate). In *NOAA Atlas NESDIS* (Vol. 84, p. 35).

GEOTRACES Intermediate Data Product Group. (2021). *The GEOTRACES intermediate data product 2021 (IDP2021)*. NERC EDS British Oceanographic Data Center NOC. https://doi.org/10.5285/cf2d9ba9-d51d-3b7c-e053-8486abc0f5fd

Hamilton, D. S., Moore, J. K., Arneth, A., Bond, T. C., Carslaw, K. S., Hantson, S., et al. (2020). Impact of changes to the atmospheric soluble iron deposition flux on ocean biogeochemical cycles in the Anthropocene. *Global Biogeochemical Cycles*, *34*(3), e2019GB006448. https://doi.org/10.1029/2019gb006448

Hamilton, D. S., Perron, M. M. G., Bond, T. C., Bowie, A. R., Buchholz, R. R., Guieu, C., et al. (2022). Earth, wind, fire, and pollution: Aerosol nutrient sources and impacts on ocean biogeochemistry. *Annual Review of Marine Science*, *14*(1), 303–330. https://doi.org/10.1146/annurev-marine-031921-013612

Hamilton, D. S., Scanza, R. A., Rathod, S. D., Bond, T. C., Kok, J. F., Li, L., et al. (2020). Recent (1980 to 2015) trends and variability in daily-to-interannual soluble iron deposition from dust, fire, and anthropogenic sources. *Geophysical Research Letters*, *47*(17), e2020GL089688. https://doi.org/10.1029/2020gl089688

Ho, T.-Y., Quigg, A., Finkel, Z. V., Milligan, A. J., Wyman, K., Falkowski, P. G., & Morel, F. M. M. (2003). The elemental composition of some marine phytoplankton. *Journal of Phycology*, *39*(6), 1145–1159. https://doi.org/10.1111/j.0022-3646.2003.03-090.x

Hopkinson, B. M., Seegers, B., Hatta, M., Measures, C. I., Greg Mitchell, B., & Barbeau, K. A. (2013). Planktonic C:Fe ratios and carrying capacity in the southern Drake Passage. *Deep-Sea Research Part II: Topical Studies in Oceanography*, *90*, 102–111. https://doi.org/10.1016/j.dsr2.2012.09.001

Howard, J. B., & Rees, D. C. (1996). Structural basis of biological nitrogen fixation. *Chemical Reviews*, *96*(7), 2965–2982. https://doi.org/10.1021/cr9500545

Hudson, R. J. M., & Morel, F. M. M. (1990). Iron transport in marine phytoplankton: Kinetics of cellular and medium coordination reactions. *Limnology & Oceanography*, *35*(5), 1002–1020. https://doi.org/10.4319/lo.1990.35.5.1002

Ito, A., Myriokefalitakis, S., Kanakidou, M., Mahowald, N. M., Scanza, R. A., Hamilton, D. S., et al. (2019). Pyrogenic iron: The missing link to high iron solubility in aerosols. *Science Advances*, *5*(5), eaau7671. https://doi.org/10.1126/sciadv.aau7671

Ito, A., Ye, Y., Yamamoto, A., Watanabe, M., & Aita, M. N. (2020). Responses of ocean biogeochemistry to atmospheric supply of lithogenic and pyrogenic iron-containing aerosols. *Geological Magazine*, *157*(5), 741–756. https://doi.org/10.1017/s0016756819001080

Jickells, T. D., & Spokes, L. J. (2001). Atmospheric iron inputs to the oceans. In *The biogeochemistry of iron in seawater, SCOR/IUPAC series* (pp. 85–121). Wiley.

Kalvelage, T., Lavik, G., Lam, P., Contreras, S., Arteaga, L., Löscher, C. R., et al. (2013). Nitrogen cycling driven by organic matter export in the South Pacific oxygen minimum zone. *Nature Geoscience*, *6*(3), 228–234. https://doi.org/10.1038/ngeo1739

Kazamia, E., Sutak, R., Paz-Yepes, J., Dorrell, R. G., Vieira, F. R. J., Mach, J., et al. (2018). Endocytosis-mediated siderophore uptake as a strategy for Fe acquisition in diatoms. *Science Advances*, *4*(5), eaar4536. https://doi.org/10.1126/sciadv.aar4536

King, A. L., Sañudo-Wilhelmy, S. A., Boyd, P. W., Twining, B. S., Wilhelm, S. W., Breene, C., et al. (2012). A comparison of biogenic iron quotas during a diatom spring bloom using multiple approaches. *Biogeosciences*, *9*(2), 667–687. https://doi.org/10.5194/bg-9-667-2012

Krishnamurthy, A., Moore, J. K., Mahowald, N., Luo, C., & Zender, C. S. (2010). Impacts of atmospheric nutrient inputs on marine biogeochemistry. *Journal of Geophysical Research*, *115*(G1), G01006. https://doi.org/10.1029/2009jg001115

Kwiatkowski, L., Aumont, O., Bopp, L., & Ciais, P. (2018). The impact of variable phytoplankton stoichiometry on projections of primary production, food quality, and carbon uptake in the global ocean. *Global Biogeochemical Cycles*, *32*(4), 516–528. https://doi.org/10.1002/2017gb005799

Lamb, K. D., Matsui, H., Katich, J. M., Perring, A. E., Spackman, J. R., Weinzierl, B., et al. (2021). Global-scale constraints on light-absorbing anthropogenic iron oxide aerosols. *Npj Climate and Atmospheric Science*, *4*(1), 1–12. https://doi.org/10.1038/s41612-021-00171-0

Lefèvre, N., & Watson, A. J. (1999). Modeling the geochemical cycle of iron in the oceans and its impact on atmospheric CO_2 concentrations. *Global Biogeochemical Cycles*, *13*(3), 727–736. https://doi.org/10.1029/1999gb900034

Liu, M., Matsui, H., Hamilton, D. S., Lamb, K. D., Rathod, S. D., Schwarz, J. P., & Mahowald, N. M. (2022). The underappreciated role of anthropogenic sources in atmospheric soluble iron flux to the Southern Ocean. *Npj Climate and Atmospheric Science*, *5*(1), 1–9. https://doi.org/10.1038/s41612-022-00250-w

Liu, Y., Moore, J. K., Primeau, F., & Wang, W. L. (2023). Reduced CO_2 uptake and growing nutrient sequestration from slowing overturning circulation. *Nature Climate Change*, *13*(1), 83–90. https://doi.org/10.1038/s41558-022-01555-7

Long, M. C., Moore, J. K., Lindsay, K., Levy, M., Doney, S. C., Luo, J. Y., et al. (2021). Simulations with the marine biogeochemistry library (MARBL). *Journal of Advances in Modeling Earth Systems*, *13*(12), e2021MS002647. https://doi.org/10.1029/2021MS002647

Mahowald, N. M., Engelstaedter, S., Luo, C., Sealy, A., Artaxo, P., Benitez-Nelson, C., et al. (2009). Atmospheric iron deposition: Global distribution, variability, and human perturbations. *Annual Review of Marine Science*, *1*, 245–278. https://doi.org/10.1146/annurev.marine.010908.163727

Mahowald, N. M., Lindsay, K., Rothenberg, D., Doney, S. C., Moore, J. K., Thornton, P., et al. (2011). Desert dust and anthropogenic aerosol interactions in the Community Climate System Model coupled-carbon-climate model. *Biogeosciences*, *8*(2), 387–414. https://doi.org/10.5194/bg-8-387-2011

Maldonado, M. T., & Price, N. M. (1999). Utilization of iron bound to strong organic ligands by plankton communities in the subarctic Pacific Ocean. *Deep-Sea Research Part II: Topical Studies in Oceanography*, *46*(11–12), 2447–2473. https://doi.org/10.1016/s0967-0645(99)00071-5

Marchetti, A., & Maldonado, M. T. (2016). Iron. In M. Borowitzka, J. Beardall, & J. Ravel (Eds.), *The physiology of Microalgae* (Vol. 6, pp. 233–279). Springer.

Marchetti, A., Parker, M. S., Moccia, L. P., Lin, E. O., Arrieta, A. L., Ribalet, F., et al. (2009). Ferritin is used for iron storage in bloom-forming marine pennate diatoms. *Nature*, *457*(7228), 467–470. https://doi.org/10.1038/nature07539

Martin, J. H., & Knauer, G. A. (1973). The elemental composition of plankton. *Geochimica et Cosmochimica Acta*, *37*(7), 1639–1653. https://doi.org/10.1016/0016-7037(73)90154-3

Matsui, H., Mahowald, N. M., Moteki, N., Hamilton, D. S., Ohata, S., Yoshida, A., et al. (2018). Anthropogenic combustion iron as a complex climate forcer. *Nature Communications*, *9*(1), 1593. https://doi.org/10.1038/s41467-018-03997-0

McKay, R. M. L., Wilhelm, S. W., Hall, J., Hutchins, D. A., Al-Rshaidat, M. M. D., Mioni, C. E., et al. (2005). Impact of phytoplankton on the biogeochemical cycling of iron in subantarctic waters southeast of New Zealand during FeCycle: Phytoplankton and the Biogeochemical Cycling of Iron. *Global Biogeochemical Cycles*, *19*(4), GB4S24. https://doi.org/10.1029/2005GB002482

Mills, M. M., Ridame, C., Davey, M., La Roche, J., & Geider, R. J. (2004). Iron and phosphorus co-limit nitrogen fixation in the eastern tropical North Atlantic. *Nature*, *429*(6989), 292–294. https://doi.org/10.1038/nature02550

Moore, C. M., Mills, M. M., Arrigo, K. R., Berman-Frank, I., Bopp, L., Boyd, P. W., et al. (2013). Processes and patterns of oceanic nutrient limitation. *Nature Geoscience*, *6*(9), 701–710. https://doi.org/10.1038/ngeo1765

Moore, J. K., & Braucher, O. (2008). Sedimentary and mineral dust sources of dissolved iron to the world ocean. *Biogeosciences*, *5*(3), 631–656. https://doi.org/10.5194/bg-5-631-2008

Moore, J. K., & Doney, S. C. (2007). Iron availability limits the ocean nitrogen inventory stabilizing feedbacks between marine denitrification and nitrogen fixation. *Global Biogeochemical Cycles*, *21*(2), GB2001. https://doi.org/10.1029/2006GB002762

Moore, J. K., Doney, S. C., Glover, D. M., & Fung, I. Y. (2002). Iron cycling and nutrient-limitation patterns in surface waters of the World Ocean. *Deep-Sea Research Part II: Topical Studies in Oceanography*, *49*(1–3), 463–507. https://doi.org/10.1016/s0967-0645(01)00109-6

Moore, J. K., Doney, S. C., & Lindsay, K. (2004). Upper ocean ecosystem dynamics and iron cycling in a global three-dimensional model. *Global Biogeochemical Cycles*, *18*(4), GB4028. https://doi.org/10.1029/2004GB002220

Moore, J. K., Fu, W., Primeau, F., Britten, G. L., Lindsay, K., Long, M., et al. (2018). Sustained climate warming drives declining marine biological productivity. *Science*, *359*(6380), 1139–1143. https://doi.org/10.1126/science.aao6379

Morel, F. M. M., Hudson, R. J. M., & Price, N. M. (1991). Limitation of productivity by trace metals in the sea. *Limnology & Oceanography*, *36*(8), 1742–1755. https://doi.org/10.4319/lo.1991.36.8.1742

Moreno, A. R., Hagstrom, G. I., Primeau, F. W., Levin, S. A., & Martiny, A. C. (2018). Marine phytoplankton stoichiometry mediates nonlinear interactions between nutrient supply, temperature, and atmospheric CO_2. *Biogeosciences*, *15*(9), 2761–2779. https://doi.org/10.5194/bg-15-2761-2018

Myriokefalitakis, S., Ito, A., Kanakidou, M., Nenes, A., Krol, M. C., Mahowald, N. M., et al. (2018). Reviews and syntheses: The GESAMP atmospheric iron deposition model intercomparison study. *Biogeosciences*, *15*(21), 6659–6684. https://doi.org/10.5194/bg-15-6659-2018

Person, R., Aumont, O., & Lévy, M. (2018). The biological pump and seasonal variability of pCO_2 in the Southern Ocean: Exploring the role of diatom adaptation to low iron. *Journal of Geophysical Research: Oceans*, *123*(5), 3204–3226. https://doi.org/10.1029/2018jc013775

Redfield, A. C., Ketchum, B. C., & Richards, F. A. (1963). The influence of organisms on the composition of sea water. In N. Hill (Ed.), *The Sea* (Vol. 2, pp. 26–77). Wiley Intersci.

Sañudo-Wilhelmy, S. A., Kustka, A. B., Gobler, C. J., Hutchins, D. A., Yang, M., Lwiza, K., et al. (2001). Phosphorus limitation of nitrogen fixation by *Trichodesmium* in the central Atlantic Ocean. *Nature*, *411*(6833), 66–69. https://doi.org/10.1038/35075041

Sarthou, G., Vincent, D., Christaki, U., Obernosterer, I., Timmermans, K. R., & Brussaard, C. P. D. (2008). The fate of biogenic iron during a phytoplankton bloom induced by natural fertilisation: Impact of copepod grazing. *Deep-Sea Research Part II: Topical Studies in Oceanography*, *55*(5), 734–751. https://doi.org/10.1016/j.dsr2.2007.12.033

Schmidt, M. A., & Hutchins, D. A. (1999). Size-fractionated biological iron and carbon uptake along a coastal to off shore transect in the NE Pacific. *Deep-Sea Research Part II: Topical Studies in Oceanography*, *46*(11–12), 2487–2503. https://doi.org/10.1016/s0967-0645(99)00073-9

Schneider, B., Engel, A., & Schlitzer, R. (2004). Effects of depth-and CO_2-dependent C: N ratios of particulate organic matter (POM) on the marine carbon cycle. *Global Biogeochemical Cycles*, *18*(2). https://doi.org/10.1029/2003GB002184

Sedwick, P. N., Sholkovitz, E. R., & Church, T. M. (2007). Impact of anthropogenic combustion emissions on the fractional solubility of aerosol iron: Evidence from the Sargasso Sea. *Geochemistry, Geophysics, Geosystems*, *8*(10), Q10Q06. https://doi.org/10.1029/2007gc001586

Séférian, R., Berthet, S., Yool, A., Palmiéri, J., Bopp, L., Tagliabue, A., et al. (2020). Tracking improvement in simulated marine biogeochemistry between CMIP5 and CMIP6. *Current Climate Change Reports*, *6*(3), 95–119. https://doi.org/10.1007/s40641-020-00160-0

Sholkovitz, E. R., Sedwick, P. N., Church, T. M., Baker, A. R., & Powell, C. F. (2012). Fractional solubility of aerosol iron: Synthesis of a global-scale data set. *Geochimica et Cosmochimica Acta*, *89*, 173–189. https://doi.org/10.1016/j.gca.2012.04.022

Sunda, W. G., & Huntsman, S. A. (1995). Iron uptake and growth limitation in oceanic and coastal phytoplankton. *Marine Chemistry*, *50*(1), 189–206. https://doi.org/10.1016/0304-4203(95)00035-p

Sunda, W. G., Swift, D. G., & Huntsman, S. A. (1991). Low iron requirement for growth in oceanic phytoplankton. *Nature*, *351*(6321), 55–57. https://doi.org/10.1038/351055a0

Tagliabue, A., Aumont, O., DeAth, R., Dunne, J. P., Dutkiewicz, S., Galbraith, E., et al. (2016). How well do global ocean biogeochemistry models simulate dissolved iron distributions? *Global Biogeochemical Cycles*, *30*(2), 149–174. https://doi.org/10.1002/2015gb005289

Tagliabue, A., Barrier, N., Du Pontavice, H., Kwiatkowski, L., Aumont, O., Bopp, L., et al. (2020). An iron cycle cascade governs the response of equatorial Pacific ecosystems to climate change. *Global Change Biology*, *26*(11), 6168–6179. https://doi.org/10.1111/gcb.15316

Tagliabue, A., Bowie, A. R., Boyd, P. W., Buck, K. N., Johnson, K. S., & Saito, M. A. (2017). The integral role of iron in ocean biogeochemistry. *Nature*, *543*(7643), 51–59. https://doi.org/10.1038/nature21058

Tagliabue, A., Mtshali, T., Aumont, O., Bowie, A. R., Klunder, M. B., Roychoudhury, A. N., & Swart, S. (2012). A global compilation of dissolved iron measurements: Focus on distributions and processes in the Southern Ocean. *Biogeosciences*, *9*(6), 2333–2349. https://doi.org/10.5194/bg-9-2333-2012

Tanioka, T., & Matsumoto, K. (2017). Buffering of ocean export production by flexible elemental stoichiometry of particulate organic matter. *Global Biogeochemical Cycles*, *31*(10), 1528–1542. https://doi.org/10.1002/2017gb005670

Tovar-Sanchez, A., Sañudo-Wilhelmy, S. A., Garcia-Vargas, M., Weaver, R. S., Popels, L. C., & Hutchins, D. A. (2003). A trace metal clean reagent to remove surface-bound iron from marine phytoplankton. *Marine Chemistry*, *82*(1), 91–99. https://doi.org/10.1016/s0304-4203(03)00054-9

Twining, B. S., Antipova, O., Chappell, P. D., Cohen, N. R., Jacquot, J. E., Mann, E. L., et al. (2021). Taxonomic and nutrient controls on phytoplankton iron quotas in the ocean. *Limnology and Oceanography Letters*, *6*(2), 96–106. https://doi.org/10.1002/lol2.10179

Twining, B. S., Baines, S. B., Bozard, J. B., Vogt, S., Walker, E. A., & Nelson, D. M. (2011). Metal quotas of plankton in the equatorial Pacific Ocean. *Deep-Sea Research Part II: Topical Studies in Oceanography*, *58*(3), 325–341. https://doi.org/10.1016/j.dsr2.2010.08.018

Twining, B. S., Baines, S. B., Fisher, N. S., & Landry, M. R. (2004). Cellular iron contents of plankton during the Southern Ocean iron experiment (SOFeX). *Deep Sea Research Part I: Oceanographic Research Papers*, *51*(12), 1827–1850. https://doi.org/10.1016/j.dsr.2004.08.007

Twining, B. S., Baines, S. B., Fisher, N. S., Maser, J., Vogt, S., Jacobsen, C., et al. (2003). Quantifying trace elements in individual aquatic protist cells with a synchrotron X-ray fluorescence microprobe. *Analytical Chemistry*, *75*(15), 3806–3816. https://doi.org/10.1021/ac034227z

Twining, B. S., Nuñez-Milland, D., Vogt, S., Johnson, R. S., & Sedwick, P. N. (2010). Variations in Synechococcus cell quotas of phosphorus, sulfur, manganese, iron, nickel, and zinc within mesoscale eddies in the Sargasso Sea. *Limnology & Oceanography*, *55*(2), 492–506. https://doi.org/10.4319/lo.2010.55.2.0492

Twining, B. S., Rauschenberg, S., Baer, S. E., Lomas, M. W., Martiny, A. C., & Antipova, O. (2019). A nutrient limitation mosaic in the eastern tropical Indian Ocean. *Deep-Sea Research Part II: Topical Studies in Oceanography*, *166*, 125–140. https://doi.org/10.1016/j.dsr2.2019.05.001

Twining, B. S., Rauschenberg, S., Morton, P. L., & Vogt, S. (2015). Metal contents of phytoplankton and labile particulate material in the North Atlantic Ocean. *Progress in Oceanography*, *137*, 261–283. https://doi.org/10.1016/j.pocean.2015.07.001

Ustick, L. J., Larkin, A. A., Garcia, C. A., Garcia, N. S., Brock, M. L., Lee, J. A., et al. (2021). Metagenomic analysis reveals global-scale patterns of ocean nutrient limitation. *Science*, *372*(6539), 287–291. https://doi.org/10.1126/science.abe6301

Volk, T., & Hoffert, M. I. (1985). Ocean carbon pumps: Analysis of relative strengths and efficiencies in ocean-driven atmospheric CO_2 changes. In *The carbon cycle and atmospheric CO_2: Natural variations Archean to present* (Vol. 32, pp. 99–110). American Geophysical Union.

Wang, W.-L., Moore, J. K., Martiny, A. C., & Primeau, F. W. (2019). Convergent estimates of marine nitrogen fixation. *Nature*, *566*(7743), 205–211. https://doi.org/10.1038/s41586-019-0911-2

Weber, T., & Deutsch, C. (2012). Oceanic nitrogen reservoir regulated by plankton diversity and ocean circulation. *Nature*, *489*(7416), 419–422. https://doi.org/10.1038/nature11357

Wu, J., & Boyle, E. (2002). Iron in the Sargasso Sea: Implications for the processes controlling dissolved Fe distribution in the ocean. *Global Biogeochemical Cycles*, *16*(4), 33-1–33-8. https://doi.org/10.1029/2001gb001453

References From the Supporting Information

Taylor, K. E. (2001). Summarizing multiple aspects of model performance in a single diagram. *Journal of Geophysical Research*, *106*(D7), 7183–7192. https://doi.org/10.1029/2000JD900719